JOURNAL OF CHEMICAL INFORMATION AND MODELING

Article

pubs.acs.org/jcim

Ligand Binding Site Identification by Higher Dimension Molecular Dynamics

Achani K. Yatawara,[†] Milan Hodoscek,[‡] and Dale F. Mierke[†,*]

[†]Department of Chemistry, Dartmouth College, Hanover, New Hampshire 03755, United States

[‡]Laboratory for Molecular Modeling, National Institute of Chemistry, Ljubljana, Slovenia

Supporting Information

ABSTRACT: We propose a new molecular dynamics (MD) protocol to identify the binding site of a guest within a host. The method utilizes a four spatial (4D) dimension representation of the ligand allowing for rapid and efficient sampling within the receptor. We applied the method to two different model receptors characterized by diverse structural features of the binding site and different ligand binding affinities. The Abl kinase domain is comprised of a deep binding pocket and displays high affinity for the two chosen ligands examined here. The PDZ1 domain of PSD-95 has a shallow binding pocket that accommodates a peptide ligand involving far fewer interactions and a micromolar affinity. To ensure completely unbiased searching, the ligands were placed in the direct center of the protein receptors, away from the binding site, at the start of the 4D MD protocol. In both cases, the ligands were successfully docked into the binding site as identified in the published structures. The 4D MD protocol is able to overcome local energy barriers in locating the lowest energy binding pocket and will aid in the discovery of guest binding pockets in the absence of a priori knowledge of the site of interaction.

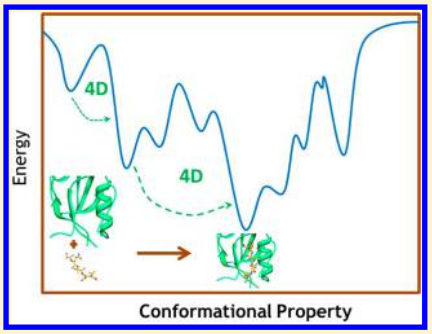

INTRODUCTION

The characterization of the specific interactions between ligands and their target proteins is essential for the rational development of molecular regulators to alter or modulate the biological function associated with the binding event. One of the first steps is the identification of the binding site of the ligand, an effort in which both experimental and theoretical methods can make essential contributions. In the absence of an experimentally determined complex structure or evidence for the site of interaction, computational methods can provide structural details and guide experimental discovery.[1−5] Standard in silico ligand-docking programs aim at predicting the preferred topological orientation of the ligand within the target receptor.[6,7] However, these docking approaches, which are generally useful in identifying key ligand/receptor interactions,[6,8] rely on knowledge of a predefined binding site within the target receptor. The search for the optimal binding mode is limited to that particular site. Our goal is to provide a robust in silico method for identifying such ligand binding sites without any prior information on the guest/host interaction. Even in those cases in which the binding site is known, the method could help in the identification of alternative binding sites (e.g., allosteric binding sites) as possible targets for intervention or drug design.

Assuming an accurate description of the potential energy of the ligand and receptor, the optimal binding site is simply defined by the lowest or global minimum energy structure of the complex. In practice, for most systems of biological interest, a complete systematic search is not feasible due to the exceeding large number of conformational variables. One common approach is to utilize molecular dynamics (MD) simulations to sample the space around discrete ligand/receptor poses.[9−11] However, during these simulations, even when carried out at elevated temperatures, the ligand is often trapped in local energy minima of the potential energy hyper surface and is unable to overcome the conformational barriers to reach its global energy minimum.[12] To overcome this obstacle, we chose to incorporate a four-spatial dimension representation of the ligand into MD simulations. The introduction of a fourth spatial dimension (4D) to a 3D object allows for quasi-tunneling through potential energy barriers during refinement of the complexes; the 4D ligand can occupy the same 3D space of the receptor, without penalty from the nonbonded terms of the force field, and therefore, the potential energy barriers present in 3D space can be evaded.[13]

Higher dimensionality has been previously utilized in energy embedding and rotational energy embedding techniques to identify energy minima.[13−16] Briefly, the molecule of N-atoms is first embedded in $(N-1)$-dimensional space so that there are no local energy minima on the potential energy surface. After energy minimization, the molecule is projected back to the next lower dimension $(N-2)$, and the cycle is repeated until the structure of the molecule in 3D is obtained. Purisima and Scheraga utilized higher dimensionality to overcome the multiple minima problem in the structure determination of the polypeptide enkephalin.[17] Introduction of a fourth spatial dimension has been employed for the refinement of structures

Received: November 26, 2012
Published: February 9, 2013

from NMR data.[18,19] The extra dimension was found to facilitate the identification of structures that fulfill all constraints derived from the experimental measurements.

Here, we examine the use of a hybrid 4D MD protocol in which the guest (the ligand) is placed in four-spatial dimensions in order to find the optimal binding site within the three-dimensional host (protein target). The 4D MD protocol was tested with three different model systems: The kinase domain of the Abl receptor was examined with two structurally diverse ligands, thiophosphoric acid o-((adenosyl-phospho)phospho)-s-acetamidyl-diester (defined as ATG) and AMN-107, for which high-resolution X-ray structures are available.[20,21] The third model is the binding of the peptide KQTSV to the PDZ1 domain of PSD-95, as determined by high-resolution NMR.[22] For this system, the binding pocket is surface exposed and very shallow and therefore more challenging to identify. We propose our method as a general in silico method for identification of previously unidentified ligand binding sites that can then be exploited in structure-based drug discovery efforts.

METHOD

The 4D MD technique was validated with three different well-defined small molecule−protein complexes. For each of the complexes, a high definition structure is available, detailing the ligand binding site characteristics. We chose the complexes formed by two small molecules, ATG (thiophosphoric acid o-((adenosyl-phospho)phospho)-s-acetamidyl-diester) (PDB ID: 2G1T_chain E and residue number 1101) and AMN-107 (PDB ID: 3CS9_chainA of residue ID NIL) (Figure 1) with

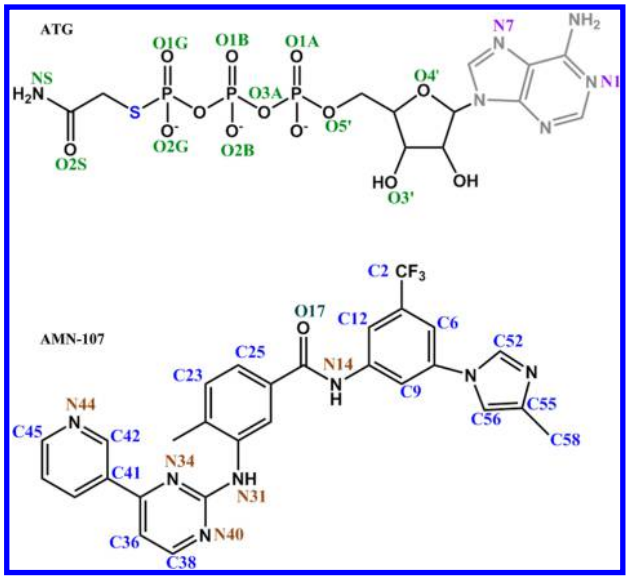

Figure 1. Molecular structures and atomic nomenclature of the small molecule ligands bound to ABl-kinase, ATG, and AMN-107.

the kinase domain of Abl (PDB ID: 2G2F_chain A) and the peptide KQTSV (PDB ID: 1BE9_chain B) with the PDZ1 domain of PSD 95 (PDB ID: 1RGR_chain A). These initial structures were cleaned by removing all extra molecules including water and then missing hydrogen atoms were added. Prior to any simulations, the ligands were removed from their binding sites.

The fourth dimensional energy embedding is introduced to the ligand as shown in eq 1. The total potential energy (U_{total}) consists of the standard CHARMM[23−25] potential energy expressions for bonded and nonbonded interactions with the addition of a harmonic energy term for the fourth dimension coordinates denoted as ω (eq 1) and a weighting constant denoted as K4D. The fourth Cartesian coordinate is added to x, y, and z coordinates of the ligand by use of the Leap Frog Verlet algorithm[26−30] (LeapFrogVerlet4D in CHARMM[23−25]). Molecular dynamics simulations are then carried out employing Newton's equations of motion (eq 2).

$$U_{total}(\vec{r}_i) = \text{Bonding Energy} + \text{Nonbonding Energy} + \sum_{i=1}^{N} \frac{1}{2}\text{K4D} \times \omega_i^2 \quad (1)$$

$$\frac{d^2\vec{r}_i(t)}{dt^2} = -\frac{1}{m_i}\frac{\partial U_{total}(\vec{r}_i)}{\partial \vec{r}_i} \quad (2)$$

where m_i is the mass of atom i and $\vec{r}_i$ is its position.

For the simulations with the Abl kinase, the CHARMM topology and parameter files were generated for the ATG and AMN-107 ligands. Beginning with the X-ray structures of the two kinase complexes, the ligand was removed far away from the binding site by orienting the center of masses of both receptor and the ligand along the x-axis. The 4D coordinate ω was introduced to the ligand coordinates while keeping the receptor coordinates in 3D. The initial 4D coordinates (ω) for the three ligands were 8.4, 8.3, and 8.7 for ATG, AMN-107, and peptide, respectively. Next, the complex was energy minimized with the steepest descent algorithm[29] (nsteps 150, step 0.02 ps) followed by the production run of the 4D molecular dynamics employing the LeapFrogVerlet4D algorithm. The K4D force constant was set to 50, and the 4D MD carried out at constant temperature at 300 K with a 1 fs time step for all three ligand−protein complexes. This procedure allows the ligand to explore the potential energy surface within the context of a fully flexible receptor. After the MD simulation, the 4D coordinates of the ligand are back-projected into 3D by gradually increasing K4D, thereby forcing the ω-coordinates to zero with the conservation of energy. For back projection, K4D was increased linearly during the simulation (increased by a factor of 150) at 300 K and kept at this value while cooling the 4D temperature from 300 to 0K with 1 fs time step. In the cases in which the dimensionality reduction produces high energy 3D structures (an inherent problem in the final step of 4D energy embedding), rotations about the principle axis of inertia before and after back projection rectified the problem.[16] The total 4D MD simulation was run for 30 and 10 ps for ATG and AMN-107, respectively, in vacuum condition with a 1 fs time step size. After the 4D simulation and back-projection, the solvated system with 10 Å water box was introduced to the ligand−protein complex system and relaxed for 200 ps (1 fs/step) using a fixed protein backbone to obtain the final ligand−receptor complex at constant temperature at 300 K. A similar procedure was used for the PDZ1−peptide complex. The peptide backbone was kept fixed to the initial structure during the 4D MD simulation (100 ps, 1 fs/step) and then released during the energy relaxation after back projection into 3D.

The results from our simulations were compared with the high-resolution (X-ray for the Abl kinase and NMR for the PDZ complex) structures available for these model systems. The root-mean-square deviations (RMSD) of the backbone atoms of the proteins were calculated (Figures 1S −5S, Supporting Information). For comparison purposes, the total

dx.doi.org/10.1021/ci300561b | J. Chem. Inf. Model. 2013, 53, 674−680

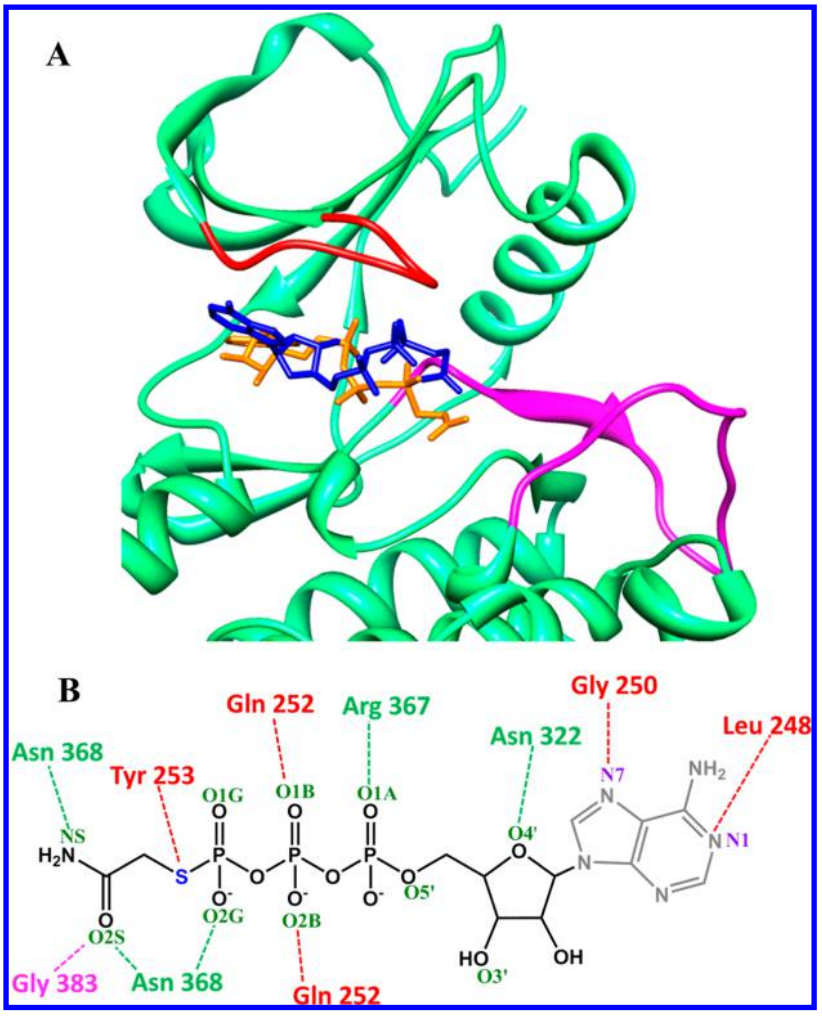

Figure 2. Abl-kinase–ATG complex. (A) Structure of the complex from the 4D MD protocol (protein green, ligand blue) superimposed with the ligand (orange) from the complex solved previously by X-ray.[20] For reference, the P-loop (residues 248–255) and activation loop (residues 381–402) are shown in red and magenta, respectively. (B) Interactions between ATG and Abl-kinase are shown schematically. Color coding of the protein amino acids indicate P-loop (red), activation loop (magenta), or other (green).

energy of the X-ray and NMR structures that were cleaned by removing other molecules including water as described above, but in this case keeping the ligand in the binding site, were calculated using the CHARMM force field and 1 ps run (2 fs/step) (Supporting Information). The difference in the total energy of experimentally determined structures and those calculated here are reported as percentages.

RESULTS AND DISCUSSION

The 4D MD procedure was successfully applied to two model receptors: (1) Abl-kinase and (2) PDZ1 of PSD95, which were chosen because of their very different characteristics of their ligand binding sites. The ligand binding pocket of the kinase domain of Abl is deep with a large number of ligand–receptor interactions.[31−35] The small molecule antagonists of Abl-kinase ATG and AMN-107 (nilotinib) (Figure 1) were examined as high-resolution structures are available, and they induce different inactive conformational states of the kinase upon binding. The peptide binding domain of the PDZ1 of PSD95 is surface exposed, shallow, and with a limited number of ligand–receptor contacts, consistent with low affinity binding associated with the physiological function of PDZ domains.[22,36−40] The pentapeptide KQTSV was used for these simulations. For three test cases, the 4D MD protocol, correctly locates the ligand binding site on the protein, both with respect to location and topological orientation, in the absence of any previous information or bias of the computational search. The agreement of the mode of binding with the experimental data is shown in Figures 2–4.

Abl Kinase and ATG. The starting structure was generated by translating the ligand to the center of the protein, 10.4 Å away from the center of the binding site. If the ligand were restricted to 3D, the large number of steric clashes between the ligand and receptor would lead to exceedingly high energies. During the 4D energy embedding protocol, the ligand moves slowly through the center of the protein to the surface, finally locating the binding site illustrated in Figure 2. The variation of distances between selected atoms of the ATG ligand and binding site during the simulation are shown in Figure 3. The ligand is within the binding site at the 200th trajectory frame (20 ps) (i.e., almost end of the 4D simulation), and during further energy relaxation in 3D, the ligand reorients itself inside the binding pocket to adopt the more energetically stable conformation as shown in Figure 2. The ligand–receptor complex reveals several interactions comparable with the published X-ray structure.[20] The ATG ligand is hydrophilic in

dx.doi.org/10.1021/ci300561b | J. Chem. Inf. Model. 2013, 53, 674–680

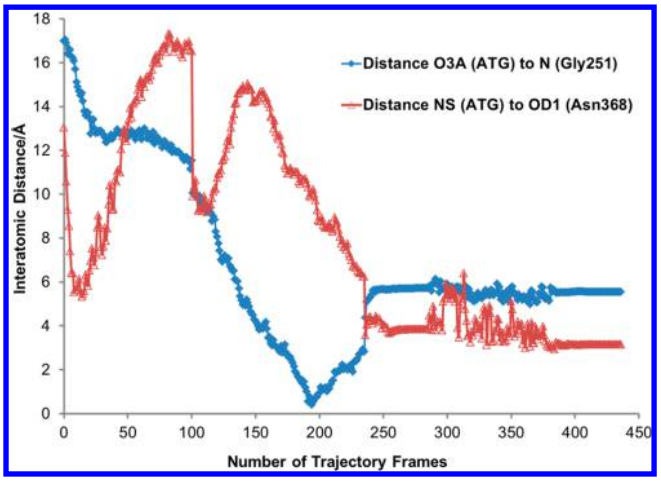

Figure 3. Variation of interatomic distances between atoms of ATG and the binding site during the simulation. The ligand reached the binding site around the 200th trajectory frame (toward the end of the 4D MD) and stayed inside the pocket throughout the simulation.

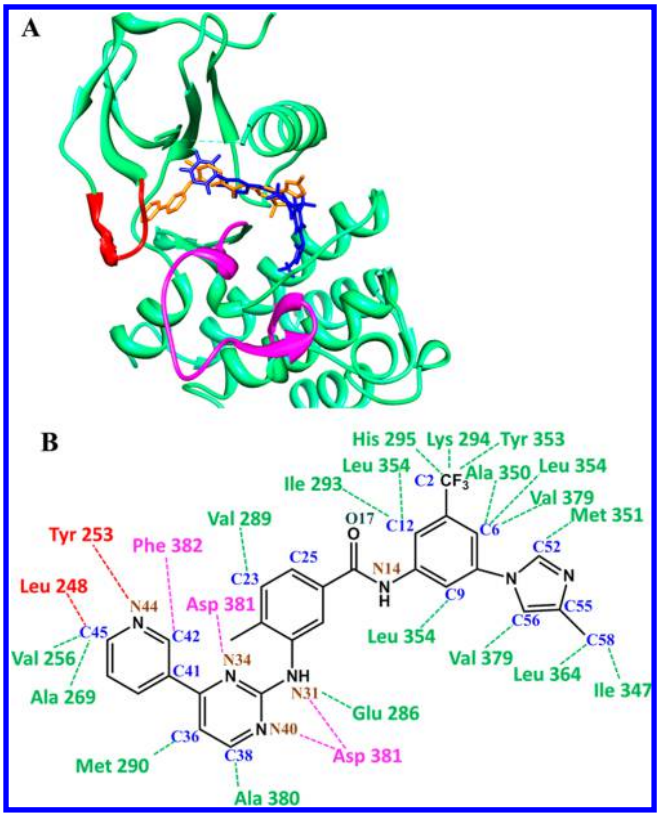

Figure 4. Abl-kinase–AMN-107 complex. (A) Structure of the complex from the 4D MD protocol (protein green, ligand blue) superimposed with the ligand (orange) from the previous determined X-ray structure.[21] For reference, the P-loop (residues 248–255) and activation loop (residues 381–402) are shown in red and magenta, respectively. (B) Interactions between AMN-107 and Abl-kinase are shown schematically. Color coding of the protein amino acids indicate P-loop (red), activation loop (magenta), or other (green).

nature and shows mainly electrostatic interactions with its host, as detailed in Table 1 and Figure 2B. The major difference from our results and the X-ray structure is the orientation of the adenine ring (Figure 2A); our simulations have the ring slightly more removed from the pocket, with more surface exposed

Table 1. Hydrophilic Interactions between ATG Ligand and Receptor

	present work		reference work[20]	
residue	atoms: receptor and ligand	distance between atoms (Å)	atoms: receptor and ligand	distance between atoms (Å)
Gln-252	NE2 and O2B	3.17	OE1 and NS	5.18
Gln-252	NE2 and O1B	3.22	–	–
Asn-368	OD1 and O2G	4.84	ND2 and O2G	5.23
Asn-368	ND2 and O2S	4.76	ND2 and O1B	3.83
Asn-368	OD1 and NS	3.15	–	–
Tyr-253	OH and S	5.44	OH and S	5.41
Leu-248	O and N1	3.22	–	–
Gly-250	O and N7	4.41	–	–
Gly-383	N and O2S	4.39	–	–
Arg-367	NE and O1A	4.87	NE and O2S	2.87[a]
Asn-322	ND2 and O4′	4.52	ND2 and O3′	2.80[a]

[a]Hydrogen bonding.

largely from interactions of the ribose with the explicit solvent. The proteins are very similar in conformation with a RMSD between the backbone atoms of the proteins of 0.57 Å. Superposition of the heavy atoms of the ligands results in a RMSD of 2.3 Å (Figure 2S, Supporting Information), demonstrating that alternative ligand conformations were sampled during the simulation. The energy of the complex system after 4D MD protocol is 6% less than the X-ray structure based on the CHARMM force field. This indicates that energy minimization beginning with the X-ray structure would lead to deviations toward the complex structure produced here.

Abl Kinase and AMN-107. Starting with the X-ray structure of the complex, the ligand was translated into the center of the protein (8.3 Å away from the binding site), and the 4D energy embedding protocol was carried out. As with ATG, the mode of AMN-107 binding as reproduced from the simulations is similar to the X-ray structure, with a number of key interactions recapitulated (Figure 4). The ligand reached the correct binding site during the 25th trajectory frame and stayed there for the remainder of the simulation (Figure 6S, Supporting Information). During the 3D MD simulation, the ligand reoriented to optimize the interactions with the receptor. In the final structure, we note a slight translation of the ligand in our structure, resulting in a more solvent exposed imidazole end of AMN-107. Despite this difference, the ligand is in the correct topological orientation within the binding pocket. The ligand is different slightly in conformation, with a RMSD of all heavy atoms of 1.7 Å (Figure 4S, Supporting Information). Some of the interactions that differ between the structures include a hydrogen bond between Glu-286 side chain with N31 (atomic labels for AMN-107 ligand are shown in Figure 1) rather than N14 observed in the X-ray structure.[21] Likewise, our structure has the carbonyl of Asp-381 interacting with N31, N40, and N34 of AMN-107, while it is the amide N atom of

dx.doi.org/10.1021/ci300561b | J. Chem. Inf. Model. 2013, 53, 674–680

Asp-381 interacting with O17 of AMN-107 ligand in the crystal. Several hydrophobic interactions involving Leu-364, Ile-347, Ala-350, Met-351, Leu-364, and Val-379 of the receptor were observed from our simulations as listed in Table 2. The energy

Table 2. Hydrophobic Interactions between AMN-107 Ligand and Receptor

	present work		reference work[21]	
residue	atoms: receptor and ligand	distance between atoms (Å)	atoms: receptor and ligand	distance between atoms (Å)
Val-256	CG1 and C45	4.01	CG1 and C38	3.93
Leu-248	CD1 and C45	6.80	CD1 and C41	3.62
Val-289	CG1 and C23	5.00	CG1 and C55	4.06
Met-290	CE and C36	3.85	CE and C25	3.92
Ile-293	CD and C12	4.31	CD1 and C6	4.39
Ala-269	CB and C45	4.66	CB and C42	4.09
Ala-350	CB and C6	3.83	–	–
Leu-354	CD1 and C9	3.60	CD1 and C12	7.94
Leu-354	CD2 and C12	3.60	–	–
Leu-354	CG and C6	3.40	–	–
Phe-382	CD1 and C42	3.93	CD1 and C38	3.37
Met-351	CE and C52	3.48	–	–
Val-379	CG1 and C56	3.44	–	–
Val-379	CG1 and C6	3.15	–	–
Ala-380	CB and C38	3.87	CB and C38	6.75
Ile-347	CG2 and C58	3.18	–	–
Leu-364	CD1 and C58	4.11	–	–

difference between the complex system after the 4D MD protocol and X-ray structure (calculated using the CHARMM force field) are comparable (a 2% difference). The very small difference in energies is consistent with the small difference in protein structures; the RMSD between the backbone atoms of the protein is 0.18 Å.

PDZ1 of PSD-95 and KQTSV. PDZ domains typically bind to the C-terminal four amino acids of its target in a short-lived transitory fashion enhancing the local concentration of the target and thereby facilitating specific protein−protein interactions. Consistent with its biological function, the PDZ1 domain of PSD-95 has a shallow hydrophobic binding pocket[22,39,40] with micromolar affinities for the peptide analogs of protein C-termini. The NMR structure of PDZ1 of PSD-95 was solved for the pentapeptide KQTSV. The starting structure was generated by moving the ligand into the center of the protein, 11.8 Å away from the center of the binding site. Even for this more challenging case, with a less well-defined binding site, the 4D MD protocol successfully identified the location of the binding pocket with the ligand in the correct topological orientation. To demonstrate the progression to the binding site, selected interatomic distances between the peptide and binding site are shown in Figure 7S of the Supporting Information. A comparison between the experimentally derived complex and the present work is shown in Figure 5. One of the key features of the PDZ domains of PSD-95 is the "GLGF" loop that binds to the C-terminus of the ligand.[22,39,40] Indeed, in our resulting complex, the carboxylic acid of the C-terminus of KQTSV

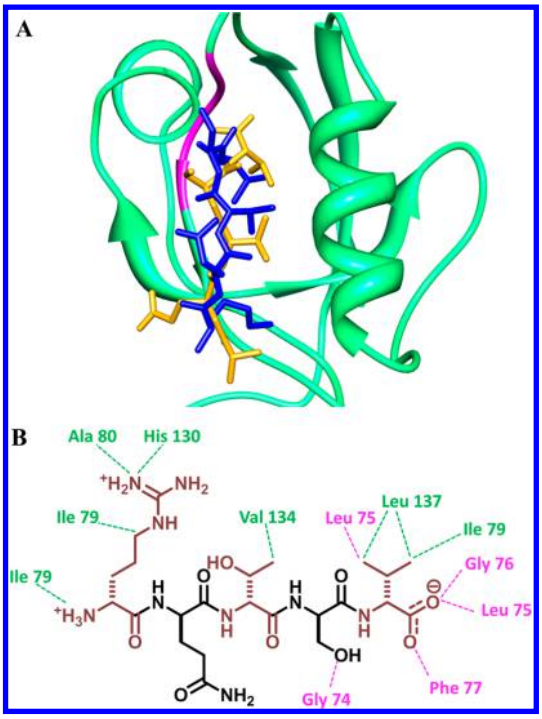

Figure 5. PDZ1 PSD-95/KQTSV complex. (A) Structure of the complex from the 4D MD protocol (protein green, ligand blue) superimposed with the ligand (orange) from the previous NMR structure.[22,39] For reference, the GLGF loop important for binding is shown in magenta. (B) Interactions between KQTSV and the PDZ1 domain are shown schematically. The interactions involving the GLGF loop are denoted by magenta and others in green.

forms a hydrogen bonding network with the amide nitrogens of Leu-75, Gly-76, and Phe-77 of the GLGF loop. Additional hydrogen bonds were observed between the Lys side chain of KQTSV and backbone carbonyl of Ala-80 and side chain of His-130. These interactions are similar to the NMR structure as well as the X-ray structure of PDZ3 of PSD-95 binding to the C-terminus of CRIPT.[39] The resulting complex from our simulations also showed several hydrophobic interactions (Table 3), consistent with the experimentally derived complex structures. The RMSD between the backbone atoms of the PDZ proteins is 0.21 Å.

Table 3. Hydrophobic Interactions between KQTSV Peptide with PDZ Domain (PSD-95)

		present work		reference work[22,39]	
residue in the receptor	residue in the ligand	atoms: receptor and ligand	distance between atoms (Å)	atoms: receptor and ligand	distance between atoms (Å)
Leu-75	Val-9	CD1 and CG2	3.86	CD2 and CB	3.56
Val-134	Thr-7	CG2 andCG2	3.44	CG2 and CG2	3.69
Leu-137	Val-9	CB and CG2	3.52	CG and CG2	4.77
Leu-137	Val-9	CD1 and CG2	3.84	–	–
Ile-79	Val-9	CD and CG1	3.51	–	–
Ile-79	Lys-5	CG1 and CD	3.54	–	–

dx.doi.org/10.1021/ci300561b | J. Chem. Inf. Model. 2013, 53, 674−680

The 4D energy embedding method[13,16,41] is a versatile technique for crossing energy barriers and identifying minima within complex energetic profiles. Here, we demonstrated that by including a 4D representation of the ligand, the ligand binding site and many of the key ligand−receptor interactions can be quickly identified. For the structurally and functionally different ligand−protein complexes examined here, the correct topological orientation of the ligand was reproduced. Of course, there are some limitations to the method. The high-resolution structure of the target receptor needs to be defined. Likewise, depending on the size and structural flexibility of the ligand, its structural features need to be defined. Often, the structure of the ligand while bound can be accessed by transferred NOEs, in absence of the complex structure. Finally, the binding event should not produce major conformational changes of the target protein. Although the receptor is fully flexible during the simulation, and therefore minor changes induced by binding will be accommodated, large conformational changes will be more difficult to identify during the MD protocol, and the identification of the ligand binding site would be much more difficult.

CONCLUSIONS

Here, we present a new MD method that utilizes 4D molecular dynamics simulations of a ligand to locate the best binding site within its target receptor. This method could prove useful in structure-based drug discovery efforts stalled by the lack of binding site information. Indeed, many small molecule screening approaches result in the identification of binders without information on the location or mode of binding to the target protein. If the structure of the target is known, then the approach outlined here will be extremely beneficial in the generation of a model of the ligand−receptor complex.

ASSOCIATED CONTENT

Supporting Information

Figures 1S−5S show the structural comparisons of the ligand−receptor complexes (ATG:Abl-kinase, AMN-107:Abl-kinase, and KQTSV:PSD-95-PDZ1) calculated in the present work and the previously published structures. Figures 6S and 7S show the convergence of the simulations for AMN107:Abl-kinase and KQTSV peptide:PSD-95-PDZ1 systems, respectively. The method used for calculation of the energies of the initial X-ray structures and a sample input script are provided. This material is available free of charge via the Internet at http://pubs.acs.org.

AUTHOR INFORMATION

Corresponding Author

*E-mail: Dale.F.Mierke@Dartmouth.edu.

Notes

The authors declare no competing financial interest.

ACKNOWLEDGMENTS

This work was supported in part by NIH Grants NS-65719 and GM-54082. We thank Dr. Maria Pellegrini and Dr. Chamila Rupasinghe for reading the manuscript and their invaluable comments. All the simulations were carried out in Dartmouth College Discovery Linux Clusters.

ABBREVIATIONS

4D MD, fourth-dimension molecular dynamics; ATG, thiophosphoric acid o-((adenosyl-phospho)phospho)-s-acetamidyl-diester; AMN-107, nilotinib

REFERENCES

(1) Congreve, M.; Murray, C. W.; Blundell, T. L. Structural biology and drug discovery. *Drug Discovery Today* **2005**, *10* (13), 895−907.
(2) Ekins, S.; Mestres, J.; Testa, B. In silico pharmacology for drug discovery: Methods for virtual ligand screening and profiling. *Br. J. Pharmacol.* **2007**, *152* (1), 9−20.
(3) Ekins, S.; Mestres, J.; Testa, B. In silico pharmacology for drug discovery: Applications to targets and beyond. *Br. J. Pharmacol.* **2007**, *152* (1), 21−37.
(4) Terstappen, G. C.; Reggiani, A. In silico research in drug discovery. *Trends Pharmacol. Sci.* **2001**, *22* (1), 23−26.
(5) Kapetanovic, I. M. Computer-aided drug discovery and development (CADDD): In silico-chemico-biological approach. *Chem. Biol. Interact.* **2008**, *171* (2), 165−176.
(6) Kuntz, I. D.; Blaney, J. M.; Oatley, S. J.; Langridge, R.; Ferrin, T. E. A geometric approach to macromolecule−ligand interactions. *J. Mol. Biol.* **1982**, *161* (2), 269−288.
(7) Lengauer, T.; Rarey, M. Computational methods for biomolecular docking. *Curr. Opin. Struct. Biol.* **1996**, *6* (3), 402−406.
(8) Morris, G. M.; Goodsell, D. S.; Halliday, R. S.; Huey, R.; Hart, W. E.; Belew, R. K.; Olson, A. J. Automated docking using a Lamarckian genetic algorithm and an empirical binding free energy function. *J. Comput. Chem.* **1998**, *19* (14), 1639−1662.
(9) Wang, J.; Dixon, R.; Kollman, P. A. Ranking ligand binding affinities with avidin: A molecular dynamics-based interaction energy study. *Proteins: Struct., Funct., Genet.* **1999**, *34* (1), 69−81.
(10) Mangoni, M.; Roccatano, D.; Di Nola, A. Docking of flexible ligands to flexible receptors in solution by molecular dynamics simulation. *Proteins: Struct., Funct., Genet.* **1999**, *35* (2), 153−162.
(11) Aqvist, J.; Medina, C.; Samuelsson, J. E. New method for predicting binding-affinity in computer-aided drug design. *Protein Eng.* **1994**, *7* (3), 385−391.
(12) Taylor, R. D.; Jewsbury, P. J.; Essex, J. W. A review of protein_small molecule docking methods. *J. Comput.-Aided Mol. Des.* **2002**, *16* (3), 151−166.
(13) Crippen, G. M. Why Energy Embedding Works. *J. Phys. Chem.* **1987**, *91* (25), 6341−6343.
(14) Crippen, G. M. Conformational analysis by scaled energy embedding. *J. Comput. Chem.* **1984**, *5* (6), 548−554.
(15) Crippen, G. M. Conformational analysis by energy embedding. *J. Comput. Chem.* **1982**, *3* (4), 471−476.
(16) Crippen, G. M.; Havel, T. F. Global energy minimization by rotational energy embedding. *J. Chem. Inf. Comput. Sci.* **1990**, *30* (3), 222−227.
(17) Purisima, E. O.; Scheraga, H. A. An approach to the multiple-minima problem in protein folding by relaxing dimensionality. Tests on enkephalin. *J. Mol. Biol.* **1987**, *196* (3), 697−709.
(18) Grdadolnik, S. G.; Mierke, D. F. Structural characterization of the molecular dimer of the peptide antibiotic vancomycin by distance geometry in four spatial dimensions. *J. Chem. Inf. Comput. Sci.* **1997**, *37* (6), 1044−1047.
(19) Vanschaik, R. C.; Berendsen, H. J. C.; Torda, A. E.; van Gunsteren, W. F. A structure refinement method based on molecular dynamics in four spatial dimensions. *J. Mol. Biol.* **1993**, *234* (3), 751−762.
(20) Levinson, N. M.; Kuchment, O.; Shen, K.; Young, M. A.; Koldobskiy, M.; Karplus, M.; Cole, P. A.; Kuriyan, J. A Src-like inactive conformation in the Abl tyrosine kinase domain. *PLoS Biol* **2006**, *4* (5), 753−767.
(21) Weisberg, E.; Manley, P. W.; Breitenstein, W.; Bruggen, J.; Cowan-Jacob, S. W.; Ray, A.; Huntly, B.; Fabbro, D.; Fendrich, G.; Hall-Meyers, E.; Kung, A. L.; Mestan, J.; Daley, G. Q.; Callahan, L.; Catley, L.; Cavazza, C.; Azam, M.; Neuberg, D.; Wright, R.; Cowan-

Jacob, S. W.; Ray, A.; Huntly, B.; Fabbro, D.; Fendrich, G.; Hall-Meyers, E.; Kung, A. L.; Mestan, J.; Daley, G. Q.; Callahan, L.; Catley, L.; Cavazza, C.; Azam, M.; Neuberg, D.; Wright, R. D.; Gilliland, D. G.; Griffin, J. D. Characterization of AMN107, a selective inhibitor of native and mutant Bcr-Abl. *Cancer Cell* **2005**, *7* (2), 129−141.

(22) Piserchio, A.; Salinas, G. D.; Li, T.; Marshall, J.; Spaller, M. R.; Mierke, D. F. Targeting specific PDZ domains of PSD-95: Structural basis for enhanced affinity and enzymatic stability of a cyclic peptide. *Chem. Biol.* **2004**, *11* (4), 469−473.

(23) Brooks, B. R.; Bruccoleri, R. E.; Olafson, B. D.; States, D. J.; Swaminathan, S.; Karplus, M. Charmm: A program for macromolecular energy, minimization, and dynamics Calculations. *J. Comput. Chem.* **1983**, *4* (2), 187−217.

(24) CHARMM c35b1. CHARMM (Chemistry at HARvard Macromolecular Mechanics). http://www.charmm.org/documentation/c35b1/charmm.html (accessed February 15, 2013).

(25) Brooks, B. R.; B., C. r.; Mackerell, A. D., Jr; Nilsson, L.; Petrella, R. J.; Roux, B.; Won, Y.; Archontis, G.; Bartels, C.; Boresch, S.; Caflisch, A.; Caves, L.; Cui, Q.; Dinner, A. R.; Feig, M.; Fischer, S.; Gao, J.; Hodoscek, M.; Im, W.; Kuczera, K.; Lazaridis, T.; Ma, J.; Ovchinnikov, V.; Paci, E.; Pastor, R. W.; Post, C. B.; Pu, J. Z.; Schaefer, M.; Tidor, B.; Venable, R. M.; Woodcock, H. L.; Wu, X.; Yang, W.; York, D. M.; Karplus, M. CHARMM: The Biomolecular Simulation Program. *J. Comput. Chem.* **2009**, *30* (10), 1545−1614.

(26) Verlet, L. Computer experiments on classical fluids .I. Thermodynamical properties of Lennard−Jones molecules. *Phys. Rev.* **1967**, *159* (1), 98−103.

(27) Hockney, R. W. In *Methods in Computational Physics*; Academic Press: New York, 1970; Vol. *9*, pp 135−211.

(28) Frenkel, D., Berend, S. *Understanding Molecular Simulation: From Algorithms to Applications*; Academic Press: New York, 1996.

(29) Leach, A. R. *Molecular Modelling Principles and Applications*, 2nd ed.; Prentice Hall: Upper Saddle River, NJ, 2001.

(30) Cuendet, M. A.; van Gunsteren, W. F. On the calculation of velocity-dependent properties in molecular dynamics simulations using the leapfrog integration algorithm. *J. Chem. Phys.* **2007**, *127* (18), 1841021−1841028.

(31) Eck, M. J.; Shoelson, S. E.; Harrison, S. C. Recognition of a high-affinity phosphotyrosyl peptide by the Src homology-2 domain of P56(Lck). *Nature* **1993**, *362* (6415), 87−91.

(32) Welch, P. J.; Wang, J. Y. J. A C-terminal protein-binding domain in the retinoblastoma protein regulates nuclear c-Abl tyrosine kinase in the cell cycle. *Cell* **1993**, *75* (4), 779−790.

(33) Manley, P. W.; Cowan-Jacob, S. W.; Mestan, J. Advances in the structural biology, design and clinical development of Bcr-Abl kinase inhibitors for the treatment of chronic myeloid leukaemia. *Biochim. Biophys. Acta* **2005**, *1754* (1−2), 3−13.

(34) Nagar, B.; Bornmann, W. G.; Pellicena, P.; Schindler, T.; Veach, D. R.; Miller, W. T.; Clarkson, B.; Kuriyan, J. Crystal structures of the kinase domain of c-Abl in complex with the small molecule inhibitors PD173955 and imatinib (STI-571). *Cancer Res.* **2002**, *62* (15), 4236−4243.

(35) Schindler, T.; Bornmann, W.; Pellicena, P.; Miller, W. T.; Clarkson, B.; Kuriyan, J. Structural mechanism for STI-571 inhibition of abelson tyrosine kinase. *Science* **2000**, *289* (5486), 1938−1942.

(36) Kim, E.; Niethammer, M.; Rothschild, A.; Jan, Y. N.; Sheng, M. Clustering of shaker-type K+ channels by interaction with a family of membrane-associated guanylate kinases. *Nature* **1995**, *378* (6552), 85−88.

(37) Kornau, H. C.; Schenker, L. T.; Kennedy, M. B.; Seeburg, P. H. Domaininteraction between Nmda receptor subunits and the postsynaptic density protein Psd-95. *Science* **1995**, *269* (5231), 1737−1740.

(38) Niethammer, M.; Kim, E.; Sheng, M. Interaction between the C terminus of NMDA receptor subunits and multiple members of the PSD-95 family of membrane-associated guanylate kinases. *J. Neurosci.* **1996**, *16* (7), 2157−2163.

(39) Doyle, D. A.; Lee, A.; Lewis, J.; Kim, E.; Sheng, M.; MacKinnon, R. Crystal structures of a complexed and peptide-free membrane protein-binding domain: Molecular basis of peptide recognition by PDZ. *Cell* **1996**, *85* (7), 1067−1076.

(40) Saro, D.; Li, T.; Rupasinghe, C.; Paredes, A.; Caspers, N.; Spaller, M. R. A thermodynamic ligand binding study of the third PDZ domain (PDZ3) from the mammalian neuronal protein PSD-95. *Biochemistry* **2007**, *46* (21), 6340−6352.

(41) Crippen, G. M., Havel, T. F. Distance Geometry and Molecular Conformation. In *Chemometrics Research Studies Series*; Bawden, D., Ed.; Research Studies Press (Wiley): New York, 1988.